INVESTIGATING THE IMPACT OF H3K27M ON CHROMOSOME TERRITORIES IN C. *ELEGANS*

FINAL RESEARCH PAPER

BACHELOR THESIS

Bachelor programme

Medical and Pharmaceutical Biotechnology

by

Felice WALLNER

Acknowledgements

Throughout the research period and writing process of this thesis, I have benefited greatly from assistance and support from my mentors, professors, scholarship institutions, friends, and family.

First, I would like to thank the Austrian Marshall Plan Foundation for supporting me financially during my time in Boston, but also for supporting me in my endeavors of undertaking a research position in the face of a global pandemic.

This thesis would not have been possible without the support of my external supervisor Dr. Yang Shi, who helped me advance in the lab and beyond, and the entire Shi Lab at the Boston Children's Hospital / Harvard Medical School. I would like to particularly thank Alan Jiao, who introduced me to his research project and was always there to discuss results (the good and the bad) and the necessary next steps. I would also like to acknowledge the Nikon Imaging Center at Harvard Medical School for their collaboration.

Many thanks also to my university internal supervisor Dr. Reinhard Klein and the other professors at the IMC University of Applied Sciences Krems, especially Dr. Barbara Entler and Dr. Harald Hundsberger, for making the opportunity of doing a semester's worth of research abroad possible, and for their support throughout.

Last, but not least, I would like to thank my friends and family for supporting me before and during my time abroad. I know that without their words of encouragement, I might not have had the bravery to start what would turn out to be a life-changing experience.

Abstract

Diffuse intrinsic pontine glioma (DIPG) is an incurable childhood brain tumor that is fatal mostly within a year of diagnosis. The majority of DIPG tumor cells carry a mutation in the gene encoding H3.3 (*H3F3A*), which leads to a lysine to methionine substitution at position 27 in the N-terminal amino acid tail (H3.3K27M) and a genome-wide decrease in trimethylation (me3) at this locus caused by an inhibition of the Polycomb Repressive Complex 2 (PRC2) histone methyltransferase activity. PRC2 and H3.3K27me3 are essential for maintaining chromatin states, as the deposition of me3 is associated with silenced chromatin and PRC2 is a known regulator of chromatin packaging. Furthermore, knockdown of the catalytic subunit of PRC2 was shown to give rise to aberrant, disorganized chromosome territories. Using whole chromosome Oligopaint FISH, we examine whether the H3K27M mutation and its effect on PRC2 impacts chromosome territories. Results show that chromosome territory volumes increase between wildtype and H3K27M mutant C. *elegans* worms under temperature stress and that there is a significant increase in both autosome and sex chromosome territory volumes in both strains. The H2K27M mutation was therefore concluded to negatively impact the integrity of chromosome territories, however, more research is necessary to elucidate further significance of this cancer phenotype.

Table of Contents

List of Illustrations

List of Abbreviations

C. *elegans*	Caenorhabditis elegans
Chr	Chromosome
DIPG	Diffuse Intrinsic Pontine Glioma
DNA	Desoxyribonucleic acid
EZH2	Enhancer of zeste homolog 2
H3	Histone 3
H3K27M	Histone 3 Lysine 27 to Methionine mutation
K	Lysine
K27M	Mutant C. *elegans* worm
L4440	Empty RNAi vector
M	Methionine
me3	trimethylation
mes3	Maternal effect sterile (gene), RNAi vector
N2	Wildtype C. *elegans* worm
Oligo	Oligonucleotide probe
pHGG	Pediatric high-grade glioma
PRC2	Polycomb repressive complex 2
PTM	Posttranslational modification
RNAi	RNA interference assay

1 Introduction

The past two decades have brought exciting new insights in the field of epigenetics (1,2). Epigenetics, translated from Greek language, means “on top of genes”. Hence, epigenetic research explores not the genetic information contained within the DNA sequence, but rather studies the branch of genetics that governs the expression of these genes encoded in the DNA sequence (3,4). Investigations of the human epigenome have revealed numerous epigenetic factors to be driving forces in human diseases, particularly in certain types of cancers. The discovery of mutations near sites of active posttranslational modification (PTM) on histones has led to the discovery of so-called “oncohistones” and the recognition for their effect on chromatin biology as an emerging hallmark of cancer (1). This thesis addresses the epigenetic factors contributing to tumorigenesis of Diffuse Intrinsic Pontine Glioma, a type of pediatric brain tumor, and how it might impact 3D genome organization, in hopes of elucidating further mechanisms behind this cancer.

1.1 3D genome organization and chromosome territories

Genetic information is stored inside the nucleus in the form of DNA, which condenses into chromatin. The most basic organization unit is the nucleosome, where DNA wraps around the histone octamer. Histones undergo various epigenetic posttranslational modifications such as methylation, acetylation and phosphorylation (5) that impact nucleosome packaging and consequently regulate DNA expression (6,7). Strings of nucleosomes form chromatin (8). The resulting chromatin fiber associates into higher order structures of different sizes: chromatin coils into loops (9) then forms topologically associated domains (TADs) and compartments (7–10)(Figure 1). The reason why genetic material is organized into these defined structures is still under active investigation, although it is probable that these structures form in order to enable different interaction profiles and transcriptional states and to contribute to genome integrity (11–13). Even interphase chromatin, which is present in a much looser form between cell divisions because DNA does not condense into

mitotic chromosomes, resides in specific parts of the nucleus according to which chromosome it belongs to (14). Aberrations in chromosome territory arrangements have been discovered to be a potent influence on gene regulation and stability in health and disease (1,14). This thesis focuses on these chromosome territories and the significance of their architectural integrity in H3K27M mutant C. *elegans* worms.

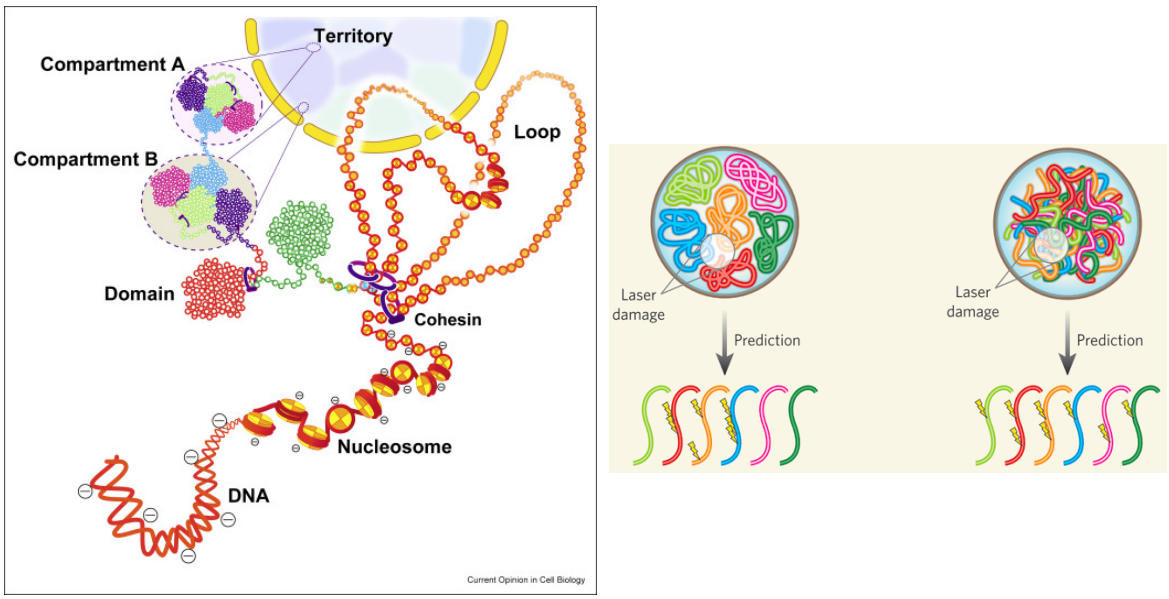

Figure 1: ***3D Chromosome Organization****.* ***Left****: Chromatin organization inside the nucleus. DNA wraps around the histone proteins, forming nucleosomes, which further condense to chromatin. Chromatin coils into loops and domains, which form compartments and organize into chromosome territores in the interphase nucleus. Adapted from Maeshima et al. 2020* (11). ***Right****: Organized vs. random chromosome organization model. Experiments by Cremer et Cremer in 1980 involving laser damage to the nucleus confirmed the organized, non-random chromosome territory model (left). Adapted from Cremer 2010* (13).

In 1885, the scientist Carl Rabl first suggested that interphase chromosomes arrange into non-random chromosome territories (14). Scientific evidence of this was procured only later in 1980, when Thomas and Christoph Cremer showed that only very specific parts of the DNA were damaged by a laser beam, supporting the theory that chromosomes are organized into territories that interact with their immediate neighbors (14–16). Since then, further aspects of chromosome territories have been discovered, for example inactive and repressed DNA arranging towards the nuclear

laminar while active DNA is situated closer to the nucleolus (12,13). How chromosomes find their place in the nucleus is still unknown, but this non-random arrangement happens primarily for functional reasons: active and repressed chromatin regions can be separated from each other and interacting genes can be brought into close proximity in order to enhance gene expression efficiency (16).

1.2 H3K27M is the driver mutation in DIPG and inhibits PRC2 activity

Histone 3 (H3) has been characterized to be an oncohistone (14), as it is affected by mutations that are known to be the major factors contributing to tumorigenesis in pediatric high-grade gliomas (pHGG) (17,18). Specifically a lysine 27-to-methionine (K27M) mutation has been identified to be the driving factor in tumorigenesis of pediatric Diffuse Intrinsic Pontine Gliomas (DIPG), which are a subtype of pediatric high-grade glioma that arise in the midline of the brain (1,19,20). Children diagnosed with this rare cancer receive a poor prognosis that seldom amounts to more than a year and to this day, there is no alternative treatment except radiation, let alone a cure (18,21). It is important to note that the histone predominantly affected by the missense mutation is the histone variant H3.3 encoded by the *H3F3A* gene. H3.3 containing nucleosomes are embedded into chromatin in a cell-cycle independent manner and is incorporated into specific euchromatin and heterochromatin sites and appears to be vital for establishing and maintaining chromatin states in development (1). For the sake of simplicity, the H3.3 variant is referred to as H3 from here on. H3K27M is caused by a heterozygous point mutation resulting in a substitution of lysine to methionine at position 27 on the N-terminal amino acid tail of histone 3 (specifically the H3.3 variant) (21,22). Consequently, the trimethylation mark (me3) deposited by the Polycomb Repressive Complex 2 (PRC2) is lost not only at this locus, but throughout the genome, which is thought to be the driving force of tumorigenesis in this cancer (1,2). H3K27M inhibits the spread of the trimethylation mark to further regions, possibly by sequestration of the histone-methyltransferase PRC2 or rather exclusion of PRC2 from H3K27M occupied chromatin regions (18,21,23).

The exact mechanisms behind the defective PRC2 function are still unclear. However, residual PRC2 activity has been reported in H3K27M positive DIPG cells and has been shown to be necessary for maintaining DIPG tumor growth by repressing differentiation in neuronal cells (21,24). The exact function of H3K27M and its downstream oncogenic function are, however, still not fully characterized.

The link between loss of polycomb protein function and chromosome territory organization can be found in PRC2's role as a regulator of chromatin architecture, as the H3K27me3 mark is known to have repressive transcriptional potential (21) (Figure 2). Trimethylation induces condensed and therefore repressed chromatin (21) and, upon mutation of lysine 27, no trimethylation mark can be deposited genome-wide and the chromatin decondenses, leading to an overall increase in transcriptional activity.

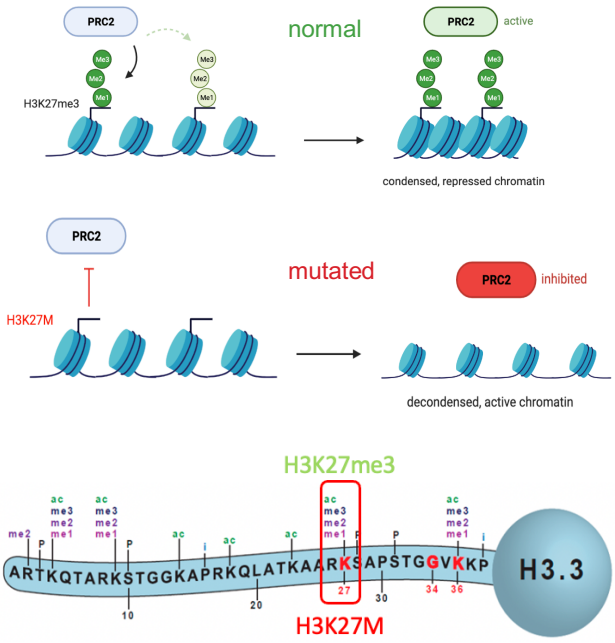

Figure 2: ***Top:*** *Schematic histone methyltransferase function of PRC2 in normal and mutated cells. In healthy cells, PRC2 is unencumbered and deposits the repressive trimethylation mark at locus H3K27. In mutated cells, PRC2 in inhibited by the H3K27M mutation in the amino acid tail and no trimethylation mark is deposited. PRC2 is inhibited from spreading me3 (or excluded from mutated chromatin, mechanisms unknown). Scheme generated in BioRender.* ***Bottom:*** *N-terminal amino acid tail of histone 3.3. PTMs at K27 marked. Green: normal trimethylation. Red: mutated lysine to methionine transition. Image adapted from Lowe et al. 2019* (25).

Furthermore, chromosomal aberrations have been shown by Fields et al. upon RNAi knockdown of *mes-3,* a gene encoding a component (EZH2) of PRC2 in C. elegans (23). Chromosome territory disorganization seen in response to EZH2 knockdown by *mes-3* RNA inference led to the conclusion that the effects of K27M on chromosome integrity may be similar, as the mutation acts inhibitory on PRC2 function. The aim was therefore to show whether the cancer inducing H3K27M mutation elicits a similar response to the effects seen after the lab induced inhibition of PRC2. While *mes-3* knockdown has previously been shown to produce prominent disorganization, chromosome territories in H3K27M mutant C. elegans have so far not been examined.

1.3 Autosomes versus sex chromosomes in H3K27M mutants

Previous RNA sequencing of the C. *elegans* H3K27M mutant epigenome showed different amounts of trimethylation loss across chromosomes (Figure 3). Upon PRC2 inhibition by H3K27M, trimethylation levels decrease on autosomes and overall RNA expression increases, while RNA expression levels on the X chromosome were shown to be reduced. Different RNA expression levels in response to a histone mutation have not been observed to date and reasons behind this are still unclear. This data provided the motive for targeting an autosome and the C. *elegans* X chromosome in our Oligopaint FISH experiments. Using FISH, the aim was to complement the RNA-seq data with a visual representation behind the effects of the H3K27M mutation on individual chromosomes and assess chromosome-wide changes of the histone mutation. It was suspected that autosome territory volumes would increase in response to the H3K27M mutation analogous to effects of knockdown with *mes-3* RNAi (25). Mutant X chromosome territory volumes were suspected to decrease in the mutant corresponding to the RNA expression profiles generated previously.

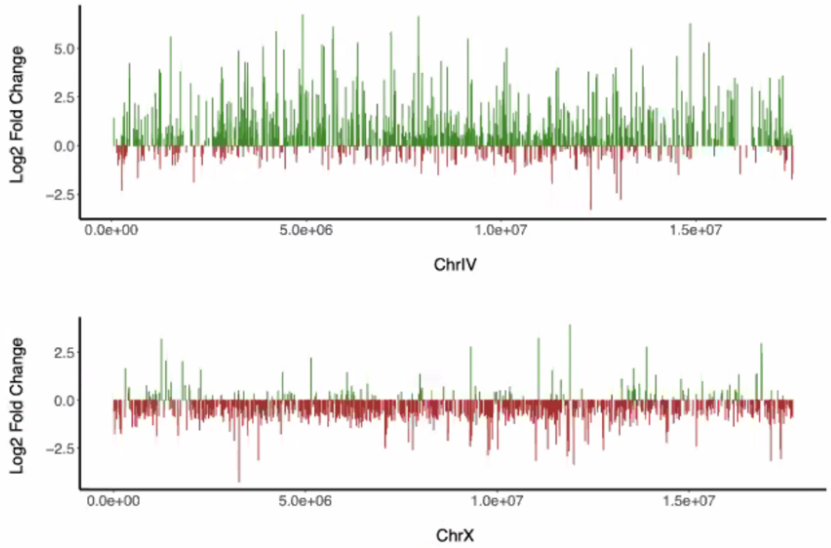

Figure 3: ***RNA-seq expression profiles of Chromosome IV and Chromosome X in C. elegans K27M mutants****. Green: positive increase in gene expression. Red: decrease in gene expression. Data provided by Alan Jiao, Shi Lab.*

1.4 Caenorhabditis elegans

The C. *elegans* worm is a small, transparent, nematode worm that is widely used for investigating questions related to basic function of eukaryotic cells, evolution, and human diseases (26,27). The concept of using C. *elegans* worms in research was proposed over 50 years ago, and it has since lead to many breakthroughs, especially in genetic studies (26). The argument for using C. *elegans* nematode worms is strongly supported by their small size, ease of cultivation and genetic manipulation, rapid life cycle, transparency, low maintenance costs, uniform cell count and established genome sequence and cell lineage (26). C. *elegans* worms pass through one life cycle, from larvae to adults, within 3-4 days. Male worms are rare, occurring at a frequency of <0.2% at optimum temperatures (20°C). Hence, most worms are self-fertilizing hermaphrodites, which is a great advantage for genetic studies, as mutant alleles in mutation screens can be preserved through self-propagation over multiple generations (26,28).

Genetic studies of C. *elegans* worms can elucidate distinct gene function by either observing the phenotype of mutant worm strains or the localization of a specific protein. Thus, many functions and even mechanisms behind specific genes have been identified using C. *elegans* (26,29). Owing to the high conservation of histone proteins and post-translational modifications between C. *elegans* and human beings, advances in worms genetics are still highly relevant in humans (30). Moreover, attaining suitable numbers of mutant worm progeny is greatly facilitated by their large brood size. CRISPR-Cas9 methods allow for the exact manipulation of a specific gene withing the endogenous genome in C. elegans worms, without the necessity of using specialized background strains that allow this manipulation (29).

Using CRISPR-based methods, our lab produced a C. *elegans* worm strain that carries a homozygotic mutation in *H3F3A. H3F3A* is one of the two genes that encode the H3.3 histone variant (the other one being *H3F3B*). However, despite similar levels of expression, only the *H3F3A* gene has been found to be affected by the H3.3K27M mutation (1,31). This induced mutation gives rise to a C. *elegans* worm strain (referred to as H3K27M or K27M worms) that shows little variance to the N2 wildtype strain at optimum temperature but reveals to be stress-sensitive at higher temperatures (25°C, 5°C above cultivation optimum), resulting in a sterility phenotype (31). The diminished brood size at 25°C has no impact on the assessment of chromosome territory volumes, as the number of progenies is still large enough to propagate for at least two generations at this temperature. H3K27M mutant chromosome territory volumes at 20°C and 25°C were compared to see whether temperature plays a role in chromosome territory volume change.

1.5 Using multiplexed DNA FISH for whole chromosome visualization

By using the novel Oligopaint FISH technology, user defined probes can be synthesized from a common pool of C. elegans oligonucleotides that target the genome either at chromosomal, 3 Mb or 500 kb level (32). For the FISH experiments conducted in the context of genome organization, a common pool of oligonucleotides that span the C. *elegans* genome at chromosomal level was used, hereby reproducing the FISH technique described by Fields (25). Oligopaint FISH allows for more versatile and cost-efficient hybridization experiments, as the oligonucleotide probe library can be synthesized via amplifications and reverse transcriptions within two days and the fluorescent detection probe is only added during the FISH hybridization procedure via barcodes, rendering the need for ordering new FISH probes for each experiment redundant (25). All in all, the chromosome-specific oligonucleotide library consists of 170 594 primary probes with a 42bp length hybridization sequence and additional barcode sequences adding up to primary probes of 150 bp in length that span one entire chromosome (32). Unlike humans, C. *elegans* nematode worms only possess six chromosomes, of which we chose to visualize three.

Multicolor fluorescent in situ hybridization (FISH) is a popular approach for detecting nuclear arrangements and gene density (13,17). For discerning how individual chromosomes are organized within the nucleus, whole-chromosome FISH is necessary. In the past, whole-chromosome FISH has been costly and time-consuming, however, the novel oligopaint technology allows for a much more rapid oligonucleotide synthesis while decreasing costs simultaneously. Oligopaint FISH is a hybridization technique that uses parallel PCR amplification from a pool of unique oligonucleotides that span the C. *elegans* genome to synthesize user defined and lab-made oligonucleotide probes that allow genome visualization at chromosome, 3Mb and 500kb level (25,33). The main advantage of the oligopaint technology compared to DNA FISH is its cost efficiency and its flexibility when designing experiments.

Oligopaint probes are oligonucleotide fragments of total 150 base pair length that cover the C. *elegans* genome and enable the localization of specific regions within the genome. It consists of a unique 42 base pair binding homology and is flanked on either side by specific barcodes that allow for easy adaptation of the experimental design and repeated amplification from the original, purchased pool, which provides an almost indefinite supply of probes (25). These barcodes specifically allow for different subsections of the C. *elegans* genome to be targeted, depending on which bridge oligo is used to append the fluorescent oligonucleotide. Most importantly, oligopaint allows for an entire chromosome to easily and cheaply be tagged and visualized (25). Figure 4 shows a schematic illustration of the oligonucleotide build and the possibilities for adding different fluorescent labels. For experiments described in this thesis, bridge oligos base paired specifically to the chromosome barcode to visualize the entirety of one chromosome with one color.

The probes contained in the initial pool of probes were designed by the Wu Lab at Harvard Medical School (https://oligopaints.hms.harvard.edu/) and kindly provided for our use. The set of oligonucleotide probes were defined using a bioinformatics pipeline that identified 42bp sequences in the C. elegans genome that are unique, have similar melting points, and lack repetitive sequences (25,34). Over 80 000 probes were suitable candidates, of which 170 594 nucleotide sequences were ultimately chosen for the library, resulting in a library that covers each C. elegans chromosome with approximately two probes per kilobase of DNA. This primary mix can be ordered and subsequently repeatedly PCR amplified to yield enough oligonucleotide probes (short: oligos) for hybridization to the C. *elegans* genome. Each unique oligo sequence is flanked by barcodes that target the C. *elegans* genome either at a chromosome, 3 Mb (Mega base) or 500 kb (kilo base) level by using specific bridge oligonucleotides that bind specifically to one of the three barcodes (25). For targeting the genome at chromosomal level, a different bridge oligonucleotide was used for each chromosome and fluorescent oligonucleotide. These fluorescent detection oligonucleotides pair with the bridge oligo and are attached to one on three fluorophores: Alexa 488 (A488), Cyanine dye 3 (Cy3) and Alexa 647 (A647).

Following the protocol by Fields et al. (25), oligonucleotide probes were synthesized by PCR amplification, T7 promoter sequence annealing, reverse transcription, and alkaline hydrolysis. This is an efficient and inexpensive synthesis, which amount to approximately two days of work (limiting step is the overnight reverse transcription). Hybridization is performed using two different mixes, the first containing the primary oligos that hybridize to select chromosomes and the second containing bridge and fluorescent oligonucleotides. Thus, as bridge oligos are only introduced after hybridization of the primary probes, they act as intermediates that allow a versatile experimental design. Figure 4 shows a scheme of different combinations of fluorescent probes. By combining two different fluorescent oligonucleotides by annealing one to the 5' and the other to the 3' oligo end, the fluorescent signal can be detected differently, similar to mixing paints on canvas. For experimetns described here, oligonucleotide primary probes were exclusively singly labeled.

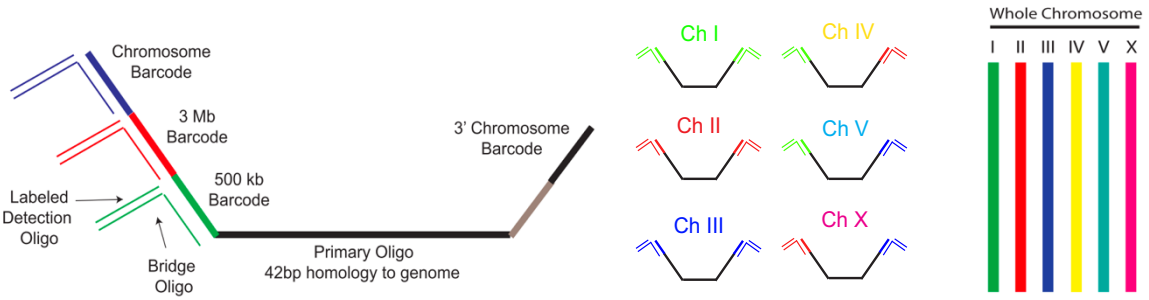

Figure 4: ***Oligopaint primary probes*** *consist of a unique 42bp hybridization sequence, which is flanked by barcode sequences. Fluorescent detection probes are appended to the specific barcode sequence via a bridge oligo, which enables flexible experiment design. Primary oligonucleotide probes with one specific fluorescent label are ultimately hybridized to the C. elegans genome to cover a whole chromosome* (25).

2 Results

2.1 Assessing DNA Oligopaint staining specificity

To test whether the Oligopaint probes only stained the specific chromosome, single-chromosome FISH samples were prepared and the germline of the C. *elegans* worm examined. Hybridization mixes without any oligonucleotide probes were also tested and showed no unexpected fluorescence. The C. *elegans* germline can be divided into sections according to the meiotic phase of the oocyte (25). For assessment of staining specificity, the pachytene region of the germline and oocytes in diakinesis was examined. Oocytes of the pachytene region are in the pachytene stage of Prophase I of meiosis, in which the homologous chromosomes (5 autosomes and one X chromosome) are present as bivalents (i.e. paired chromosomes) and should be able to be visualized as a single distinct spot which corresponds to the chromosome stained (35). The C. *elegans* worm was FISH stained with Oligopaint probes targeting chromosomes I and X in individual samples. Confocal images showed staining of only a single bivalent per nucleus in the pachytene region in both samples for chromosome I and X, indicating that our library set was specific (Figure 5). Moreover, FISH staining oocytes in their most separated phase of meiosis, namely diakinesis, revealed extremely specific signal corresponding to only one of six DAPI stained regions. No bleed-through of fluorescent signal was seen in the other channels, indicating that the dyes (A488), (Cy3) and (A647) can be used within one sample without any interference of fluorescent signals.

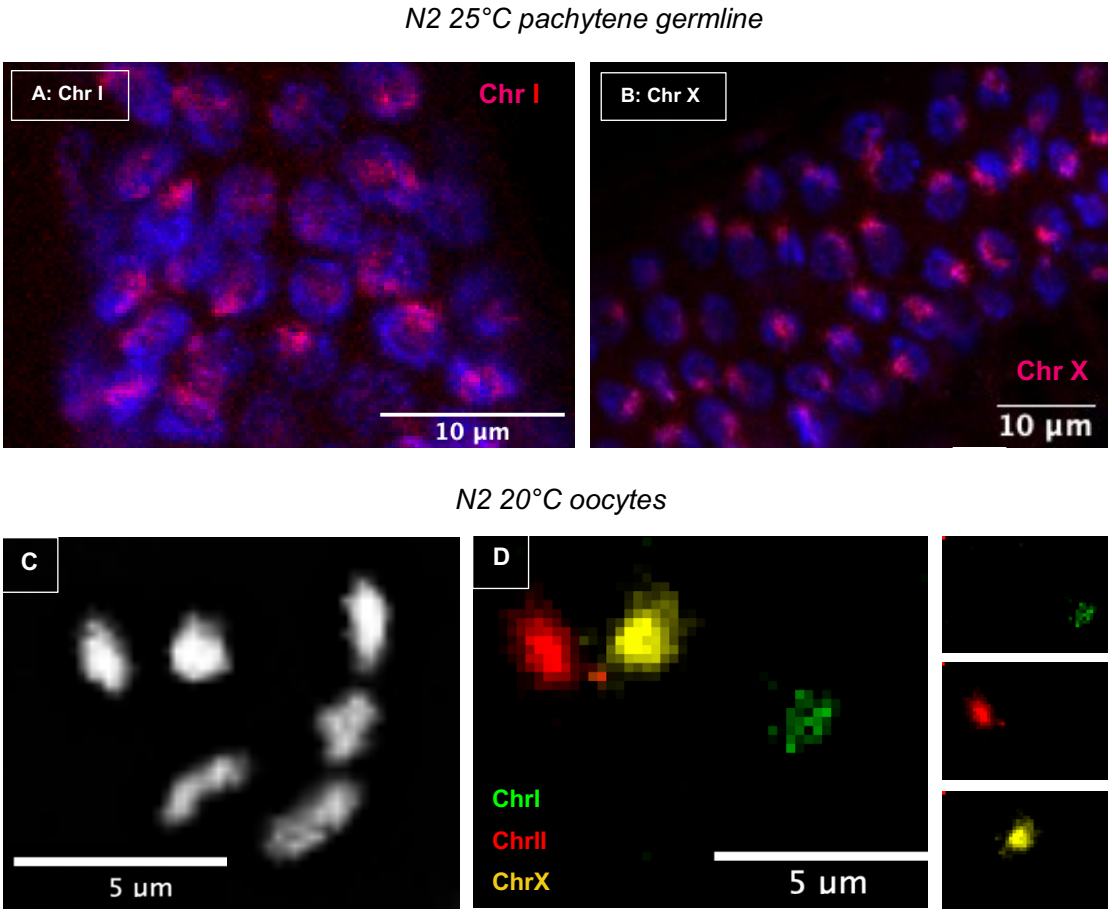

Figure 5: ***Whole chromosome FISH specificity in C. elegans germline.*** *Adult wildtype C. elegans worms (maintained at 25°C) were fixed and hybridized as described in Materials and Methods and co-stained with DAPI.* ***A&B:*** *Z-stack (~0.25µm) of the pachytene germline region. A: Cy3 red = chromosome I. B: Cy3 red = chromosome X.* ***C:*** *Adult N2 20°C oocyte visualization with DAPI. Shows the nucleus in diakinesis stage of prophase I. Six chromosome territories visible corresponding to the number of chromosomes present in a C. elegans nematode.* ***D:*** *Oocyte shown with chromosome specific FISH. Green A488 = Chr I, Red Cy3 = Chr II, Yellow A647 = Chr X. FISH is specific to one chromosome territory and no overlap of signal is observed. Scale bars as indicated. Images are representative of at least five independent animals.*

2.2 Visualizing chromosome territories using DNA FISH

To address chromosome territory volume changes across wildtype and H3K27M mutated worms, Oligopaint FISH was used to target multiple chromosomes at once and visualize them under a three-channel confocal microscope. At most, three different chromosomes (I, II, X) were targeted simultaneously, representing 50% of

total chromosome number, as C. *elegans* worms possess only six chromosomes. For chromosome territory volume assessment and comparison, only the whole worm FISH procedure was used, while the dissected FISH protocol by Fields et al. (36) was only used initially for testing the DNA accessibility for our FISH probes. Different cell types can easily be visualized within the C. *elegans* worm. There is reason to believe that chromosome territory volumes of different cell types might behave differently, which, however, is not evaluated here. We exclusively chose to analyze intestinal nuclei because they are the easiest to visualize as the largest nuclei in the C. *elegans* worm. The difference in size compared to other cell types arises due to their polyploid nature, which is a result of repeated endoreduplications during the larval worm stage (25,37).

The Oligopaint protocol allows for visualization of chromosome territories in different colors in order to address how they change in the mutant C. elegans worm compared to the wildtype (N2). C. elegans were maintained at different temperatures (20°C and 25°C) and collected according to the whole worm FISH protocol and subjected to FISH. Two different temperatures were compared due to the temperature-dependent phenotype in H3K27M worms. Mutant C. elegans show reduced fertility when maintained at a temperature-stress of 25°C (above the 20°C optimum) (31,38). C. elegans worms were imaged under the confocal microscope and analyzed with FIJI. We used the Oligopaint technique to ask whether changes in chromosome territory volumes are temperature dependent and whether a significant difference can be seen between wildtype (N2) and mutant (H3K27M) worms. The data shows that there is no difference in N2 chromosome territory volumes, but volumes increase in the mutant phenotype at elevated temperatures, confirming the temperature sensitive mutant phenotype. Chromosome I, while included in the imaging process, was not used for quantification, as C. *elegans* intestine auto-fluoresces at the same wavelength as the A488 detection oligo probe, preventing the ImageJ thresholding tool from eliminating the background properly.

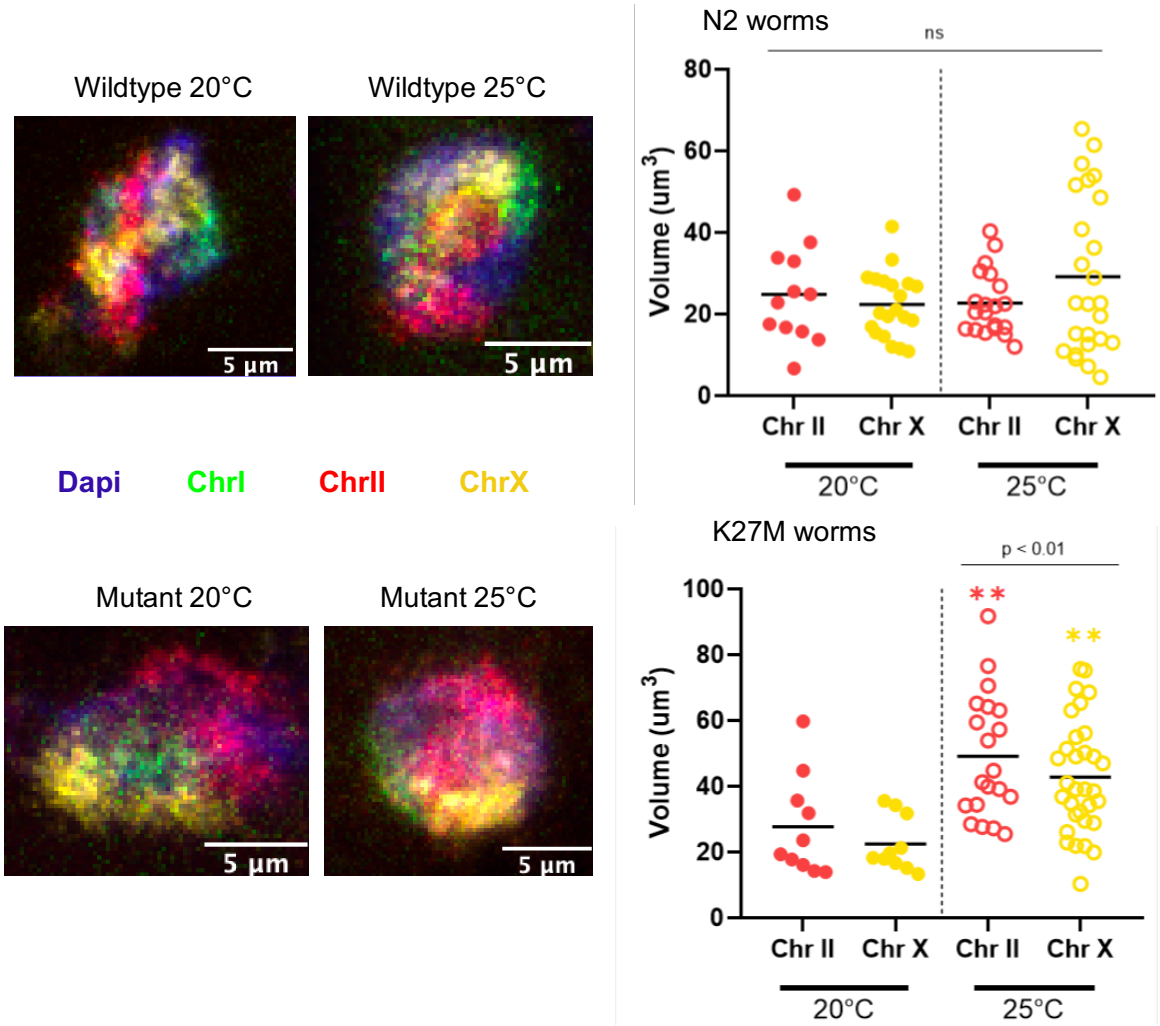

Figure 6: ***Whole worm FISH for Wildtype and Mutant C. elegans****. Top: Wildtype adult intestinal nuclei. Quantification of wildtype nuclei (excluding DAPI and Chromosome I measurements shows no significant difference between chromosome territory volumes. Bottom: Mutant adult intestinal nuclei. Quantification of mutant nuclei show a significant increase in chromosome territory volume for chromosomes II and X. p-value = 0.05. Datapoints are representative of at least three independent worms.*

To ask whether there is a change in chromosome territory volumes between N2 and K27M worms, we compared the data from N2 and K27M worms (Figure 7) and show that chromosome territory volumes seem to increase significantly at temperatures of 25°C. The mutant does not show an increase in volume at 20°C, indicating that the mutant phenotype may be activated only at higher and less optimal temperature conditions.

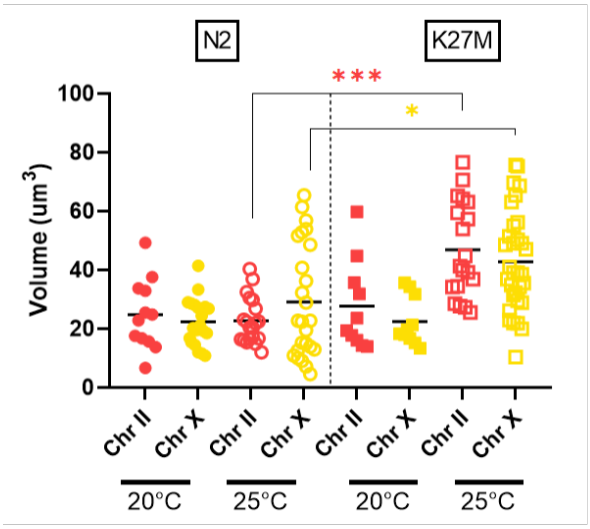

Figure 7: ***Comparison of whole worm FISH data for N2 wildtype and K27M mutant C. elegans worms****. Chromosomes II and X at 25°C show a significant increase in territory volume, while the significant is greater in the autosome than in the sex chromosome. p-value = 0.05. Datapoints are representative of at least three independent worms.*

2.3 RNA interference with *mes-3*

To compare the extent of chromosome territory degradation, a control using *mes-3* RNA interference was conducted. *mes-3* encodes EZH2, the catalytic subunit of the Polycomb Repressive Complex 2 (PRC2), the enzyme responsible for depositing the trimethylation mark at H3K27M, and is known to play a key role in maintaining chromosomal architecture (25,39). Adult C. *elegans* worms were maintained at 25°C on L4440 (E. coli lacking *mes-3* dsRNA for interference) and *mes-3* RNAi bacterial plates for two generations before collecting worms for FISH analysis. RNA interference in wildtype worms showed a loss of chromosomal territory integrity and a significant increase in territory volume in all chromosomes as a consequence of losing PRC2 function. Interestingly, chromosome territory volume increase is significantly more pronounced in the RNAi samples than in the mutant phenotype, suggesting that H3K27M worms might preserve some PRC2 activity and therefore are able to retain partial genome integrity. *mes-3* RNAi in K27M worms resulted in a loss of chromosome territory integrity similar to N2 *mes-3* RNAi.

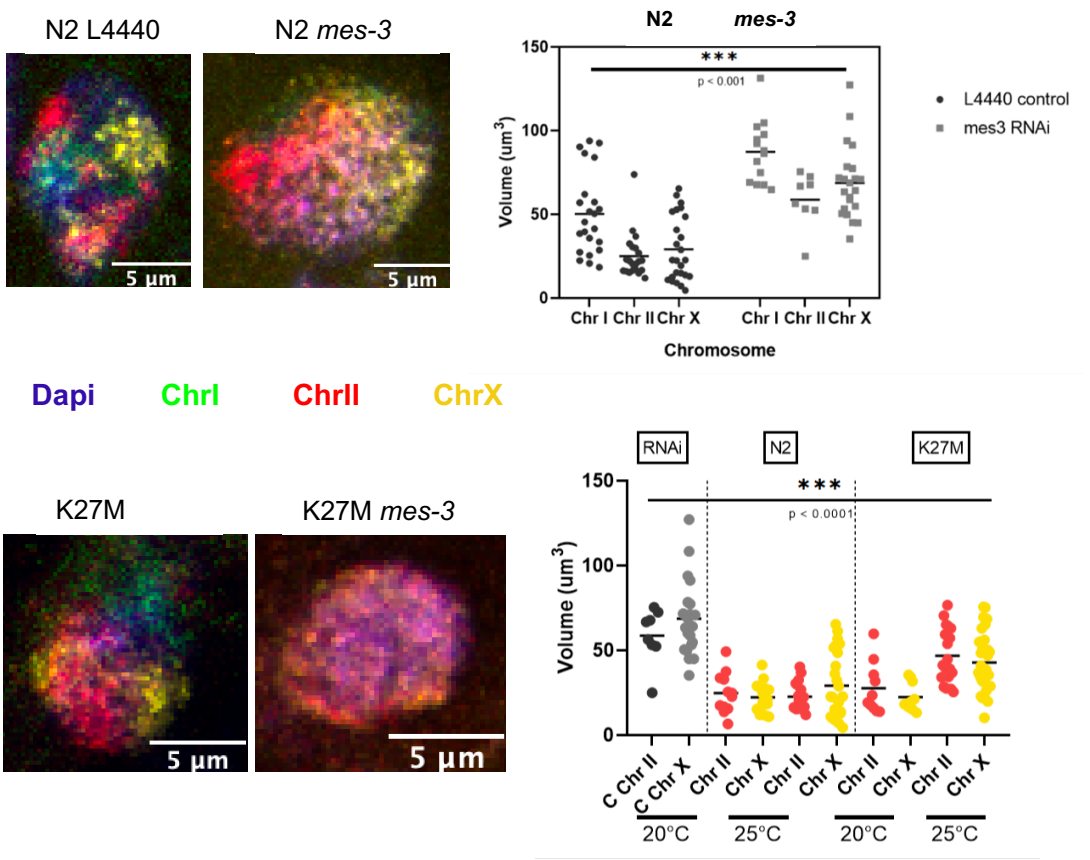

Figure 8: ***Whole worm FISH on adult C. elegans wildtype worms targeting mes-3.*** ***Top:*** *RNAi of adult wildtype C. elegans worms. Results show an increase in all chromosome territory volumes in negative control L4440 and mes3. L1 worms were placed on RNAi plates and propagated for two generations. Bottom: RNAi experiment images of K27M mutant nuclei. Note: no measurement for chromosome 1 included in K27M mes-3. Comparison of N2 and K27M territory volumes with positive N2 RNAi controls. Data is representative of at least 5 independent animals. p-value = 0.05.*

2.4 Fluorescent in situ hybridization in other C. *elegans* cell types

2.4.1 Germline

The oligo FISH technique is capable of staining all nuclei in an undissected, intact worm (40). While quantification of chromosome territory volumes was performed using large intestinal nuclei, chromosome territories were also observable in other cell types, such as oocytes, neuronal and hypodermal cell nuclei. As germline cells mature into oocytes and pass from the pachytene to the diplotene and diakinesis

stage of late Prophase I, the chromosomes condense in preparation for metaphase I and can be visualized in the C. *elegans* germline as six well-separated bivalents corresponding to the expected six chromosomes (25,41).

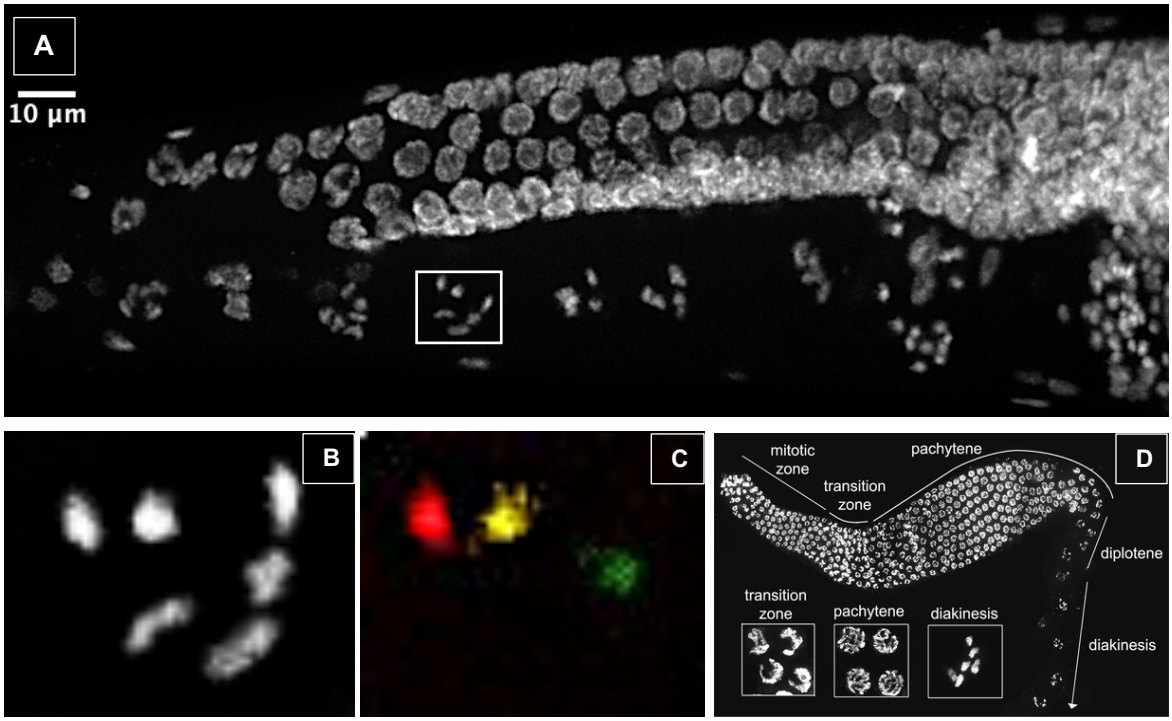

Figure 9: ***Fluorescent in situ hybridization of oocytes****.* ***A****: Grayscale DAPI stained germline (left arm of germline tube). Z-stack projection at maximum intensity with automatic brightness and contrast adjustment tool in FIJI. Germline cells seen in pachytene through diakinesis phases of meiosis I. Increased number of smaller, concentrated DAPI signals show the spermatheca of the hermaphrodite. Oocyte chosen for FISH depiction framed. Scale bar as indicated.* ***B****: DAPI grayscale projection (automatic adjustment tool of brightness and contrast) shows six highly condensed chromosomes, corresponding to the correct number expected in C. elegans worms.* ***C****: FISH-stained oocyte. Red = Chromosome II, Yellow = Chromosome X, Green = Chromosome I. Z-stack projection at automatic adjustment tool of brightness and contrast. No chromosome territory overlaps between different chromosomes, all chromosomes exist as highly condensed, separated bivalents. All images representative for n > 5 different nuclei in an adult wildtype worm. Magnification 60x.* ***D****: Picture adapted from Lui, D. (2013)* (30)*. Germ cells in the germline can be assigned their respective stages of meiosis according to their location within the gonad arm. As the germ cell passes through the tube towards the vulva, the gametes mature to oocytes.*

Figure 9 (C–D) shows an oocyte in diakinesis stage of prophase I, where homologous chromosomes are condensed to their maximum extent before separation. Staining specificity of the Oligopaint FISH probes can once again be seen by the

fluorescent oligonucleotides binding only to one of the condensed chromosomal regions. Images in Figure 9 are representative of wildtype N2 worms. Germlines of K27M mutated worms (Figure 10) appeared to not only be visually more disorganized in the mitotic and pachytene regions, but also no oocytes were distinguishable in K27M 25°C and as in the control *mes-3* worms.

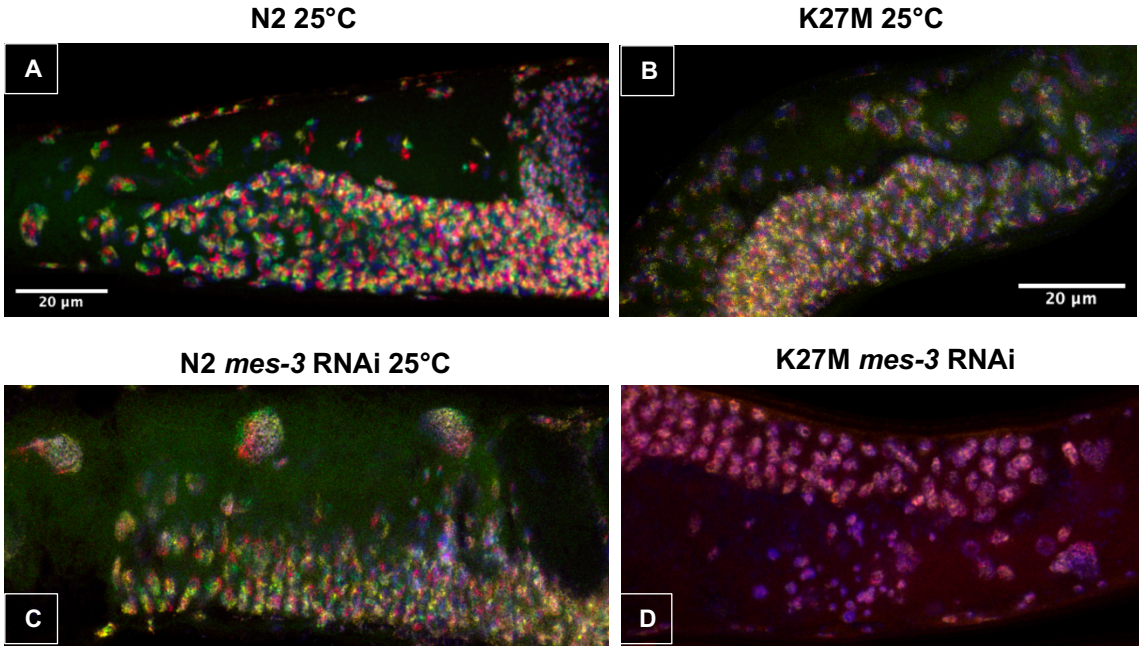

Figure 10: ***Fluorescent in situ hybridization of (pachytene) germlines****. Fluorescent signals A-C: Chr I green, Chr II red, Chr X yellow. D: Chr I red, Chr X yellow. DAPI blue for A-D* ***A:*** *N2 25°C germline tube. Chromosome territories are clearly distinguishable throughout the germline and oocytes recognizable before spermatheca.* ***B:*** *K27M 25°C mutant germline tube. Fluorescent signal is less defined to specific regions and oocytes appear abnormal. Seen analogously in Figure 5, chromosome territory volumes significantly increase in mutant worms from 20°C to 25°C. Moreover, autofluorescence (green) of the worm is higher at the elevated temperature.* ***C:*** *N2 wildtype worm RNAi with mes-3 at 25°C. Germline fluorescent signal and size seem to be less defined and diminished. Oocytes distinguishable, dark circle lacking fluorescent signal is presumably a fertilized embryo that has already passed the spermatheca. Elevated autofluorescence following elevated temperature conditions or mes-3 knockdown.* ***D:*** *K27M RNAi with mes3 at 25°C. Chr I A488 dye not included in experimental run through. Increased autofluorescence signal can be seen analogously with red signal. Germline seems less substantial, and no oocytes are distinguishable. This conforms with diminished brood size seen in K27M RNAi worms. Scale bars as indicated. Images are representative of n > 5 replicates.*

2.4.2 Neurons

The *Caenorhabditis elegans* somatic nervous system of an adult hermaphrodite is comprised of 282 neurons (42,43). The location of each neuron and synapse is reproducible to a large extent and, despite its compact nature, the C. *elegans* worm is capable of displaying several different behaviors (42,44), which are subject to extensive behavioral research. Confocal images of C. *elegans* worms showed that Oligopaint FISH also allowed the staining of motor neuronal cells throughout the worm. Specifically, D-type motor neurons, which are GABAergic type neurons contributing to locomotion (45), were easily visualized. However, chromosome volumes of motor neuron nuclei were not quantified, as their difference in size compared to the large intestinal nuclei posed as a challenge for adequate resolution and differentiation of territory areas. Figure 11 shows that motor neurons are positioned along the ventral nerve cord along the length of the worm on one side of the body.

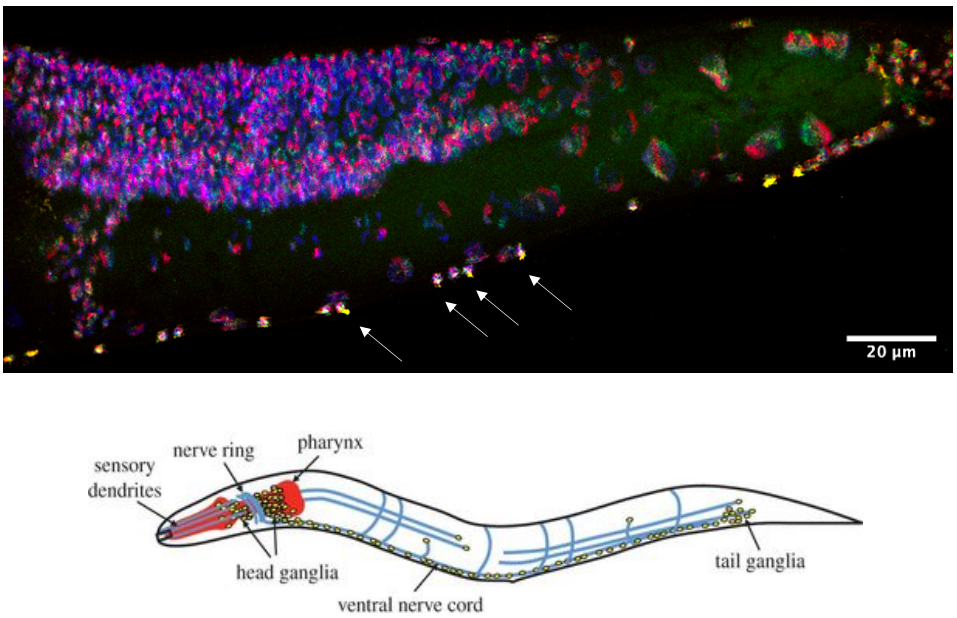

Figure 11: ***C. elegans somatic nervous system - motor neurons. A:*** *Three channel confocal image of the tail-end of an adult hermaphrodite wildtype worm. White arrows indicate motor neurons grouped along the ventral nerve cord. Scale bars as indicated.* ***B:*** *Schematic depiction of the C. elegans nervous system. Image from Fang-Yen, 2015, Illuminating neural circuits and behavior in Caenorhabditis elegans with optogenetics.*

3 Discussion

Caenorhabditis elegans worms are an excellent model organism for genetic and epigenetic studies, due to the high conservation of the histone proteins and the associated post-translational modifications between C. elegans and humans (30). Additionally, nematode worms do not demand high costs for handling and are quickly and easily propagated. C. *elegans* are naturally self-fertilizing hermaphrodites, where males (X0) occur only very infrequently, and therefore leads to genetically identical progeny (27,46). This enables easy maintenance of lab generated CRISPR mutant strains, in our case H3K27M mutants with a homozygous mutation in *H3F3A* (47).

C. elegans go through the four larval stages to adulthood within 3 days, if incubated at an optimum temperature of 20°C (27). No significant difference in life span or fertility was seen between wildtype and mutant worm at 20°C. However, it was observed that the K27M strain would demand slightly less frequent splitting than the wildtype strain when propagated simultaneously over multiple generations, presumably due to a slightly smaller brood size of the mutant worm and perhaps also due to a slight delay in growth. The introduction of the H3K27M mutation into the worms strain produces a temperature sensitive phenotype, resulting in a reduced fertility of mutant hermaphrodite worms at 25°C (27,31), seen by the diminished or lacking germ line (Figure 10). Due to this stress-induced sterility phenotype, we examined whether chromosome territories behave differently in mutant worms at 20°C and 25°C. While wildtype worms do not show an increase in chromosome territory volume, chromosome territory volumes of K27M mutant worms significantly increase when the worm is maintained at higher temperatures for more than one generation (Figure 6). This is compatible with the observation that wildtype and mutant worms show no real differences in vitality and fertility at 20°C and suggests that a temperature shift might be necessary to see the effects of the mutation in the worm phenotype.

The Oligopaint FISH technology is a fast, versatile and cheap way for visualizing DNA inside the nucleus (25,39,48). By following the protocol by Fields et al., we were able to visualize intact C. *elegans* nuclei, instead of performing FISH on dissected worms, where intestine and germline tubes spill out and the integrity of the worm's morphology is lost. Imaging cells in the intact worm facilitates comparison of cell types between biological replicates, as C. *elegans* anatomy consists only of roughly 1000 somatic cells and developmental mapping has made it possible to trace each cell to its progenitor (27,49). The primary oligonucleotide probes can be synthesized quickly by PCR amplification and reverse transcription reactions in the lab. The fluorescent molecule is only added to the oligonucleotide in the hybridization step via bridge oligos, which allows for a cheap, flexible and versatile experimental design by omitting the need to purchase new oligonucleotides whenever the need arises to amend the protocol (25,28). While the Oligopaint primary probes are capable of hybridizing to two different fluorophores and emitting a different color by mixture of the two signals, we only used three fluorophores (A488, Cy3 and A647) in our experiments. One drawback we encountered was the high autofluorescence in C. *elegans* intestine, which fluoresces on the same wavelength as A488. This autofluorescence can be reduced if the worms are kept at optimum conditions (20°C and no periods of starvation), which however was not possible in this case, since examining chromosome territories at 25°C and RNA interference represented an integral part of the experiments. As a result, quantifications of chromosome I, which we tagged with green probes from the beginning, were not able to be included in the analysis, as the background was too high to reliably quantify signal in our targets.

A difficulty encountered in the beginning procedures with Oligopaint FISH concerned the design behind labeling the primary oligonucleotides with fluorescent oligonucleotides. Fluorescent oligonucleotides used by Fields et al. were purchased from IDT (see Methods 4.3). Primarily, we used fluorescent oligonucleotides from Thermo Fisher and discovered no probe-related fluorescent signal in our sample. We concluded, after comparing the oligonucleotide designs by each company, that double-labeling of the oligo is indispensable for proper signal and that probes purchased from Thermo Fisher, which were only 3' labeled, did not produce any signal

at normal concentrations. Follow-up FISH experiments comparing both probes showed that almost 10x the amount of single-labeled fluorescent oligonucleotide was necessary in the hybridization mixture to obtain similar fluorescent signals.

While this thesis exclusively describes Oligopaint FISH in intact C. *elegans* worms, other hybridization methods were also undertaken, yet discontinued due to inferior results. Fields et al. also describe FISH on dissected C. *elegans* worms, which was superior in eliminating autofluorescence from germline visualization, but was abandoned due to time reasons and the loss of integrity of the worms' morphology. Oligopaint FISH can also be performed on C. *elegans* eggs by freeze cracking. Unfortunately, the percentage of FISH fluorescently labeled eggs was too low to efficiently assess chromosome territories. The whole-worm FISH protocol yielded the highest number of stained worms within one sample, as the FISH was done in tubes with 10µl worm pellets instead of on a glass slide, where only a few worms were fixed, and many were washed off during the procedure.

Single probe FISH of chromosome I and X with Cy 3 was performed to examine binding specificity to a single chromosome and bleed through between the channels. Quantifications of chromosome territory volumes of the multiple tagged nuclei corresponded to the values of the single-labeled sample, which verified that multiple Oligopaint probes can be used within one sample.

The reason behind choosing chromosomes I, II and X for these FISH experiments lies in previous observations of RNA-seq expression profiles of C. elegans chromosomes by the Shi Lab (). Upon the loss of PRC2 and genome-wide trimethylation levels at the H3K27 loci, gene expression levels appear to go up in the autosomes, but not in the sex chromosome. Using Oligopaint FISH, we aimed to supplement the RNA-seq data by visually comparing autosome versus sex chromosome territory volumes. Comparisons of N2 and K27M volumetric data at 25°C (Figure 7) show

that autosomal chromosome territory volumes appear to increase more than X chromosome territory volumes, implying that chromosome X is impacted to a lesser extent. Differences in RNA expression levels between autosomes and sex chromosomes has never been observed before in any cancer phenotype and indications for its cause or consequence has not yet been identified. More investigation would be necessary to confidently come to a conclusion on this point.

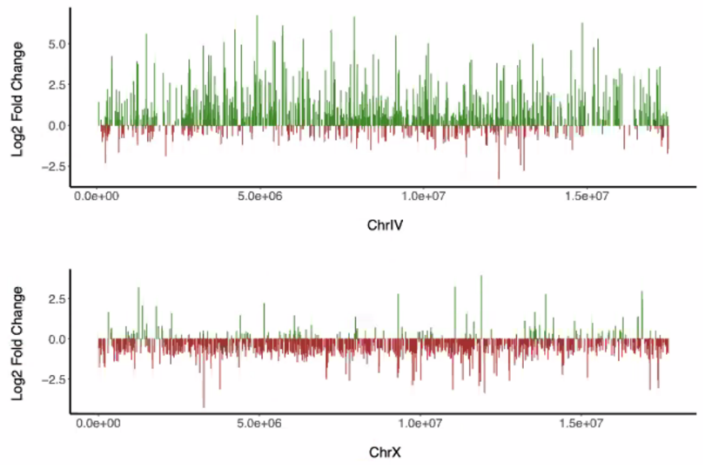

Figure 12: ***RNA-seq expression profiles of Chromosome IV and Chromosome X in C. elegans K27M mutant worms****. Green: positive increase in gene expression. Red: decrease in gene expression. Data provided by Alan Jiao, Shi Lab.*

The Oligopaint FISH technology provides an optimal approach to whole chromosome visualization. However, a limitation persists when interested in visualizing smaller loci, for example at a single gene resolution. The smallest loci able to be visualized with these oligonucleotides are 500kb long. The *mes-3* gene, for example, has a coding sequence length of approximately 2000 nucleotides (50), which is much shorter than the 500kb oligonucleotide probe. Visualizing the differences in chromatin packaging near specific genes presents another aspect that may be of interest in chromatin biology and cancer, for which, however, other approaches would need to be implemented.

In conclusion, our data shows: First, a significant increase in K27M chromosome territory volumes from 20 to 25°C conditions. Second, a significant increase in chromosome territory volumes between N2 and K27M at 25°C. Lastly, a larger increase in chromosome volumes for X than for II. FISH allows us to shed some light on the 3D organization of the genome and may give more insight to the multi-faceted mechanisms behind cancers with driving oncohistone functions. This data suggests that there is yet another molecular aspect of this cancer that needs investigating to create a more holistic picture of cancers with H3K27M mutations.

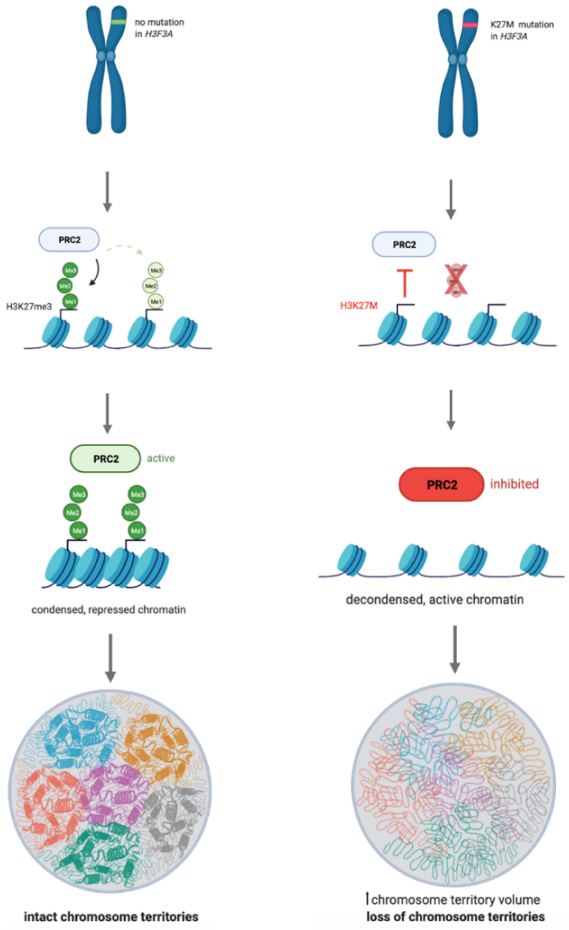

Figure 13: ***Schematic depiction of the effects of the H3K27M mutation on chromosome territories****. WT H3FA allows the spread of the me3 mark and condensation of chromatin at the desired regions. Chromosomal territory architecture is therefore intact, and territories can be distinguished with Oligopaint FISH under the confocal microscope. In the mutant genotype, H3K27M prevents trimethylation at this locus and inhibits the spread of the PRC2-deposited me3 mark. Chromatin is therefore decondensed and chromosome territory volume increases and appears disorganized under the microscope. Diagram created with Biorender.*

The next steps in examining cancer chromosome territory volumes would include performing whole chromosome DNA FISH in patient derived DIPG cells to verify that chromosome territory disorganization is not exclusive to nematode species. While recent studies have shown that chromatin in single-celled organisms forms clusters of a few nucleosomes, higher eukaryotes will form much larger clusters and more complex compartments (11). Promising future directions for assessing chromosome territories include combining Oligopaint FISH with other techniques such as chromosome conformation capture and Hi-C. Hi-C generates interaction profiles between smaller chromatin domains, such as topologically associated domains (TADs), and can therefore determine regions of chromatin that often lie in close proximity or are even connected, such as enhancers and promotors (7,51). In conclusion, examining chromatin conformations and chromosome territories are an emerging approach to understanding the fluidity of our genomic material and applying this knowledge to other diseases where regulators of chromosomal architecture, such as PRC2 in DIPG, play a significant role in tumorigenesis.

4 Materials and Methods

4.1 Key Resources:

Table 1: Key resources table

Reagent, strain or resource	Designation	Source or reference	Additional information & Identifiers
Strain, C. *elegans*	N2 (wild type)	Caeno-rhabditis Genetics Center (CGC)	https://cgc.umn.edu/strain/N2
Strain, C. *elegans*	H3K27M	Shi Lab, un-published	N/A
Strain, E. *coli*	OP50	Caeno-rhabditis Genetics Center (CGC)	https://cgc.umn.edu/strain/OP50
Genetic reagent, E. *coli*	HT115(DE3), RNAi control	Caeno-rhabditis Genetics Center (CGC)	https://cgc.umn.edu/strain/HT115(DE3)
Genetic reagent, E. *coli*	RNAi *mes-3* clone	Caeno-rhabditis Genetics Center (CGC)	N/A

4.2 Synthesis of multiplexed DNA FISH library

Primary oligonucleotide probes were synthesized using the protocol as described by Fields et al. (25). Chosen oligonucleotide probes were specific to the C. elegans genome (build ce10). Chromosome specific primary oligonucleotide probes with a total length of 150 bp (42 bp hybridization sequence plus ~54 bp barcode sequences

appended to either end) were PCR amplified using primers specific to the chromosome barcode to expand the single stranded DNA probes. A T7 promotor region was added to the 5' end of the barcode to generate ssRNA in an overnight T7 polymerase reaction at 37°C and then reverse transcribed into ssDNA. The resulting sample was purified through alkaline hydrolysis to remove remaining RNA and the single stranded oligonucleotide probes purified using the Zymo Oligo Clean & Concentrator Kit (Cat.# D4060, Lot # 206255). Probes were stored at -20°C.

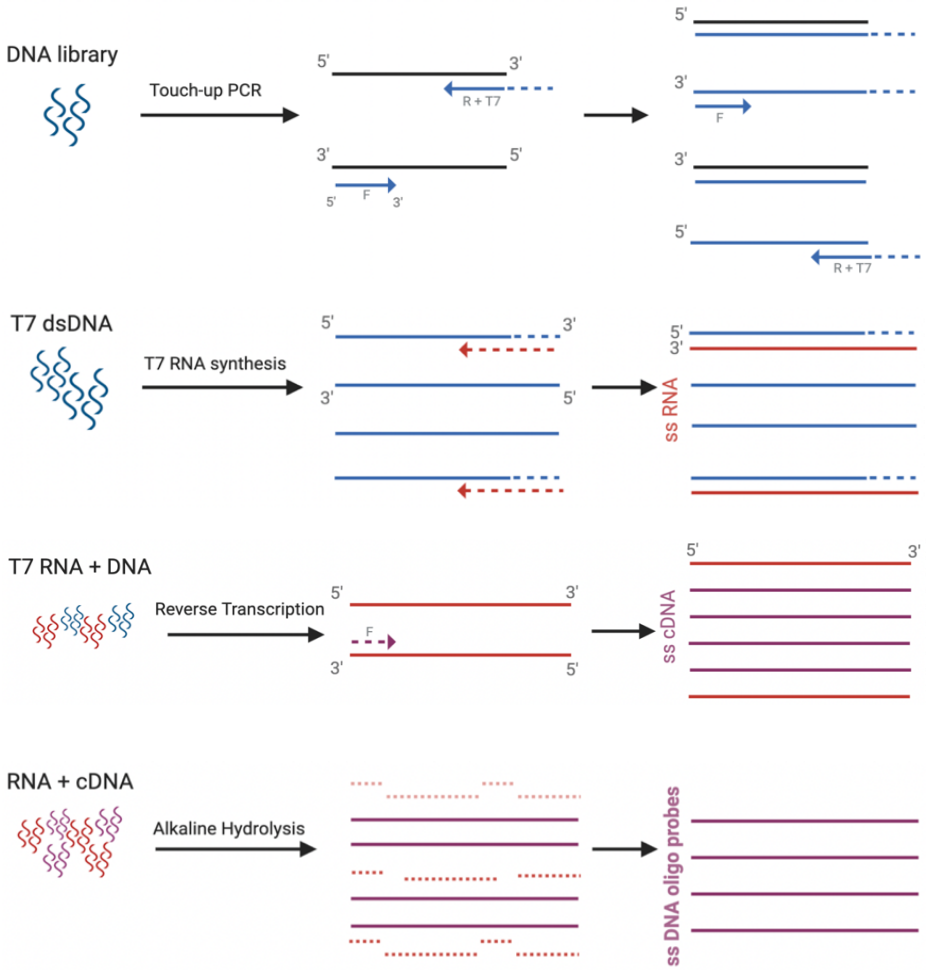

Figure 14: ***Scheme of step-by-step synthesis of ssDNA oligonucleotide probes.*** *Primary probes are synthesized from a pre-existent library first with multiple rounds of PCR, creating thousands of basic library copies. A T7 promoter sequence is appended to the probe. In an overnight reaction, T7 RNA is transcribed to ss cDNA and ultimately purified to yield ss DNA oligonucleotide probes. Scheme created using BioRender.*

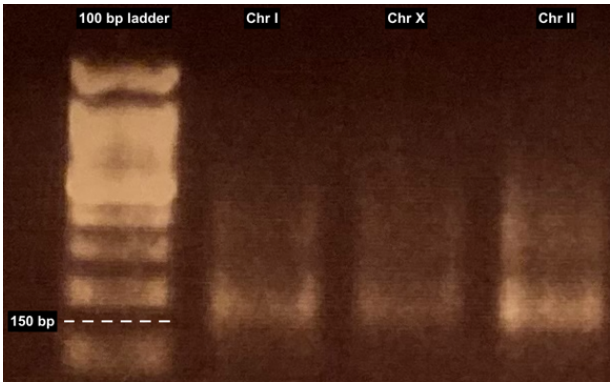

Figure 15: ***Gel electrophoresis of ss cDNA*** *(after reverse transcription and before alkaline hydrolysis). Expected length 150bp seen in three lanes of unpurified sample. Difference in band intensity due to different amplification efficiencies and T7 dsDNA concentrations in samples.*

4.3 DNA FISH in C. *elegans*

Bridge oligos were ordered from ThermoFischer and stored at 100 nmol/µl concentrations. Fluorescent detection probes were ordered from IDT with fluorescent labels (either A488, Cy3, A647) at both 5' and 3' ends. Non-starved, mixed population C. *elegans* worms were washed from 10cm plates with M9 + Triton (3 g KH2PO4, 6 g Na2HPO4, 5 g NaCl, 1 ml 1 M MgSO4, H2O to 1 liter, + 1 ml 25% Triton X) into 1.5 ml Eppendorf tubes. Worms were pelleted and washed twice more. Approximately 30 µl worm pellets aliquoted in tubes were frozen in liquid nitrogen and stored at -80°C. Whole worm fluorescent in situ hybridization was performed as described by Fields et al. (25). For the hybridization procedure, worm pellets were resuspended in 95% ethanol and vortexed on high speed for 1 minute to break up the cuticle, then rotated at room temperature for an additional 9 minutes. Samples were centrifuged (3000 rpm for 15s), supernatant aspirated and washed twice with 1 x PBST (50 ml 10x PBS, 10 ml 25% Triton X, H_2O to 500 ml). The resulting pellet was resuspended in formaldehyde fix solution (4% paraformaldehyde end conc., 4 ml 10x PBS, 26ml dH_2O) and rotated at room temperature for 6 minutes. The fixation solution was then removed and washed twice with 1 x PBST. The pellet was resuspended in 2x SSC (50 ml 20x SSC (Cat.# 51205, Lot # 0000813937), H2O to 500 ml) for 5 minutes

without rotation. Without washing the worm pellet after removing the SSC, 50% formamide in 2x SSC were added to the tube and left at room temperature for 5 minutes, before being transferred to a 95°C heat block for 3 minutes followed by 20 minutes at 65°C. The supernatant was removed as best as possible and the pellet resuspended in 60 µl primary hybridization mix (containing 100 pmol of each primary probe, 2 µl RNAse A, 30 µl formamide, 15 µl hybridization solution (400 g/L dextran Sulfate, 20ml 20x SSC, 250 µl Tween-20, dH_2O) and dH_2O). The sample was mixed well and transferred to a 100°C heat block for 5 minutes before being placed horizontally inside a 37°C incubator overnight (at least 12 hours). Next day, warm (~50°C) 2x SSCT (50ml 20x SSC, 10ml 25% Triton, H_2O to 500 ml) was added to the worms/hybridization mix, spun down, aspirated, and resuspended in 2x SSCT and rotated for 5 minutes in a 60°C incubator. The mixture was spun down, the supernatant removed, and the pellet resuspended in warm 2x SSCT and rotated for 20 minutes at 60°C. The mixture was spun down and aspirated twice to ensure no residual wash was left before resuspending in 60 µl of the bridge/detection oligo hybridization mix (100pmol of each bridge structure (5' and 3' end bridge per oligonucleotide), 100 pmol of each detection oligo, 18 µl formamide, H_2O to up to 60 µl) and left in the dark at room temperature for 3 hours. After incubation, the mixture was spun down and aspirated, and resuspended in warm 2x SSCT at 60°C for 5 minutes. This wash was repeated twice more for 20 minutes and 5 minutes respectively, where DAPI (10% concentration) stain was included in the last wash. The sample was spun down and as much excess as possible removed before being mounted on a microscope slide (ProLong™ Diamond Antifade Mountant,Ref.# P36970, Lot # 2296784).

4.4 RNAi assay

Wild-type (N2) and mutant (K27M) worms (first larval stage) were collected and placed on RNAi plates (NGM plates with 2.5 mM KH_2PO_4 and 1 mM IPTG) seeded with HT115 carrying the L4440 vector expressing *mes-3* dsDNA (control with non-*mes-3* targeting HT115 E.*coli*) for two generations before collected for FISH analysis. Worms were collected as previously described.

4.5 Microscopy

FISH-stained worms were imaged using a Nikon A1R point scanning confocal on an inverted Nikon TI microscope with a Nikon A1 plus camera and using the NIS Elements acquisition software at the Harvard Medical School Nikon Imaging Center. A 60x Plan Apo Oil objective was used. Z-stack images (0,2-0,3 µm) were obtained from whole, young adult – adult worms that showed homogenous staining throughout the whole worm.

4.6 Assessing chromosome territory volumes

Chromosome territory volumes were assessed following the protocol by Fields et al. All quantifications were performed using ImageJ with the 3D objects counter plugin (25). The multichannel (one channel representing a fluorophore bound oligonucleotide probe specific to a chromosome) z-stack image was split according to color and the “auto-thresholder” tool used on the stack with the brightest signal to remove background. The 3D objects counter tool was used to filter out objects larger than 30 voxels, hereby removing more background and creating an objects map, which was put into the 3D Manager plugin. The 3D Measure tool was used to determine the volume of each merged chromosome object map, resulting in a list of chromosome territory volumes within a nucleus.

List of References

1. Weinberg DN, Allis CD, Lu C. Oncogenic mechanisms of histone H3 mutations [Internet]. Vol. 7, Cold Spring Harbor Perspectives in Medicine. Cold Spring Harbor Laboratory Press; 2017 [cited 2021 Apr 24]. Available from: /pmc/articles/PMC5204328/

2. Kasper LH, Baker SJ. Emerging functions of histone H3 mutations in paediatric diffuse high-grade gliomas. Neuropathol Appl Neurobiol [Internet]. 2020 Feb 1 [cited 2021 Apr 24];46(1):73–85. Available from: /pmc/articles/PMC7174136/

3. Weinhold B. Epigenetics: the science of change. Environ Health Perspect [Internet]. 2006 [cited 2021 Mar 22];114(3). Available from: /pmc/articles/PMC1392256/

4. Zoghbi HY, Beaudet AL. Epigenetics and human disease. Cold Spring Harb Perspect Biol [Internet]. 2016 Feb 1 [cited 2021 Mar 22];8(2):1–28. Available from: http://cshperspectives.cshlp.org/

5. Epigenetics [Internet]. [cited 2021 Mar 22]. Available from: https://www.genome.gov/genetics-glossary/Epigenetics

6. Bannister AJ, Kouzarides T. Regulation of chromatin by histone modifications [Internet]. Vol. 21, Cell Research. Nature Publishing Group; 2011 [cited 2021 Mar 30]. p. 381–95. Available from: www.cell-research.com

7. Alberts B, Johnson A, Lewis J, Morgan D, Raff M, Roberts K, et al. Molecular Biology of the Cell. 6. editon. Garland Science; 2015. 1342 p.

8. Weinberg RA. The Biology of Cancer. Second edi. Garland Science, Taylor & Francis Group, LLC; 2014. 876 p.

9. Finn EH, Pegoraro G, Brandão HB, Valton AL, Oomen ME, Dekker J, et al. Extensive Heterogeneity and Intrinsic Variation in Spatial Genome Organization. Cell [Internet]. 2019 Mar 7 [cited 2020 Oct 7];176(6):1502-1515.e10. Available from: /pmc/articles/PMC6408223/?report=abstract

10. Yadav T, Quivy JP, Almouzni G. Chromatin plasticity: A versatile landscape that underlies cell fate and identity [Internet]. Vol. 361, Science. American Association for the Advancement of Science; 2018 [cited 2021 Feb 27]. p. 1332–6. Available from: http://science.sciencemag.org/

11. Maeshima K, Tamura S, Hansen JC, Itoh Y. Fluid-like chromatin: Toward understanding the real chromatin organization present in the cell. Curr Opin Cell Biol. 2020 Jun 1;64:77–89.

12. Boettiger AN, Bintu B, Moffitt JR, Wang S, Beliveau BJ, Fudenberg G, et al. Super-resolution imaging reveals distinct chromatin folding for different epigenetic states. Nature [Internet]. 2016 Jan 21 [cited 2020 Oct 27];529(7586):418–22. Available from: https://pubmed.ncbi.nlm.nih.gov/26760202/

13. Cremer T, Cremer M. Chromosome territories. Cold Spring Harb Perspect Biol. 2010;2(3):1–22.

14. Meaburn KJ, Misteli T. Cell biology: Chromosome territories. Nature. 2007;445(7126):379–781.

15. Misteli T. Chromosome territories: The arrangement of chromosomes in the nucleus. Nat Educ. 2008;1(1):167.

16. Finn EH, Misteli T, Shachar S. Painting a Clearer Picture of Chromatin [Internet]. Vol. 36, Developmental Cell. Cell Press; 2016 [cited 2020 Oct 27]. p. 356–7. Available from: http://dx.

17. Lowe BR, Maxham LA, Hamey JJ, Wilkins MR, Partridge JF. Histone H3 mutations: An updated view of their role in chromatin deregulation and cancer. Cancers (Basel). 2019;11(5):1–24.

18. Harutyunyan AS, Krug B, Chen H, Papillon-Cavanagh S, Zeinieh M, De Jay N, et al. H3K27M induces defective chromatin spread of PRC2-mediated repressive H3K27me2/me3 and is essential for glioma tumorigenesis. Nat Commun. 2019;10(1).

19. Sarthy JF, Meers MP, Janssens DH, Henikoff JG, Feldman H, Paddison PJ,

et al. Histone deposition pathways determine the chromatin landscapes of h3.1 and h3.3 k27m oncohistones. Elife. 2020;9:1–18.

20. Wan YCE, Liu J, Chan KM. Histone H3 Mutations in Cancer. Curr Pharmacol Reports. 2018;4(4):292–300.

21. Piunti A, Hashizume R, Morgan MA, Bartom ET, Horbinski CM, Marshall SA, et al. Therapeutic targeting of polycomb and BET bromodomain proteins in diffuse intrinsic pontine gliomas. Nat Med [Internet]. 2017 Apr 1 [cited 2021 Mar 30];23(4):493–500. Available from: /pmc/articles/PMC5667640/

22. Mosaab A, El-Ayadi M, Khorshed EN, Amer N, Refaat A, El-Beltagy M, et al. Histone H3K27M Mutation Overrides Histological Grading in Pediatric Gliomas. Sci Rep [Internet]. 2020 Dec 1 [cited 2021 Mar 30];10(1):1–9. Available from: https://www.nature.com/articles/s41598-020-65272-x

23. Silveira AB, Kasper LH, Fan Y, Jin H, Wu G, Timothy I, et al. H3.3 K27M Depletion Increases Differentiation and Extends Latency of Diffuse Intrinsic Pontine Glioma Growth In Vivo. Acta Neuropathol. 2020;137(4):637–55.

24. Shi Y, Wang XX, Zhuang YW, Jiang Y, Melcher K, Xu HE. Structure of the PRC2 complex and application to drug discovery. Acta Pharmacol Sin. 2017;38(7):963–76.

25. Fields BD, Nguyen SC, Nir G, Kennedy S. A multiplexed dna fish strategy for assessing genome architecture in caenorhabditis elegans. Elife. 2019;8:1–17.

26. Corsi AK, Wightman B, Chalfie M. A Transparent window into biology: A primer on Caenorhabditis elegans. WormBook. 2015;1–31.

27. Altun, Z.F. and Hall DH. Introduction. In: WormAtlas. 2009.

28. Pazdernik N, Schedl T. Introduction to germ cell development in caenorhabditis elegans [Internet]. Vol. 757, Advances in Experimental Medicine and Biology. Springer Science and Business Media, LLC; 2013 [cited 2021 Mar 31]. p. 1–16. Available from: /pmc/articles/PMC3781019/

29. Dickinson DJ, Goldstein B. CRISPR-based methods for caenorhabditis

elegans genome engineering. Genetics [Internet]. 2016 Mar 1 [cited 2021 May 18];202(3):885–901. Available from: /pmc/articles/PMC4788126/

30. Lui DY, Colaiácovo MP. Meiotic development in Caenorhabditis elegans. In: Germ Cell Development in C elegans Advances in Experimental Medicine and Biology [Internet]. Springer Science and Business Media, LLC; 2013 [cited 2021 Apr 20]. p. 133–70. Available from: https://link.springer.com/chapter/10.1007/978-1-4614-4015-4_6

31. Delaney K, Mailler J, Wenda JM, Gabus C, Steiner FA. Differential expression of histone h3.3 genes and their role in modulating temperature stress response in caenorhabditis elegans. Genetics. 2018;209(2):551–65.

32. Beliveau BJ, Boettiger AN, Avendaño MS, Jungmann R, McCole RB, Joyce EF, et al. Single-molecule super-resolution imaging of chromosomes and in situ haplotype visualization using Oligopaint FISH probes. Nat Commun. 2015;6(May).

33. Beliveau BJ, Apostolopoulos N, Wu CT. Visualizing genomes with oligopaint FISH probes. Curr Protoc Mol Biol [Internet]. 2013 [cited 2020 Nov 9];105(SUPPL.105):14.23.1. Available from: /pmc/articles/PMC3928790/?report=abstract

34. Beliveau BJ, Joyce EF, Apostolopoulos N, Yilmaz F, Fonseka CY, McCole RB, et al. Versatile design and synthesis platform for visualizing genomes with Oligopaint FISH probes. Proc Natl Acad Sci U S A. 2012;109(52):21301–6.

35. Phillips CM, McDonald KL, Dernburg AF. Cytological analysis of meiosis in Caenorhabditis elegans. Methods Mol Biol [Internet]. 2009 [cited 2021 Mar 27];558:171–95. Available from: /pmc/articles/PMC3644504/

36. Riddle DL, Blumenthal T, Meyer BJ, Priess JR. Meiosis. In: C elegans II [Internet]. 2nd editio. Cold Spring Harbor Laboratory Press; 1997 [cited 2021 Mar 27]. Available from: https://www.ncbi.nlm.nih.gov/books/NBK20188/

37. Hedgecock EM, White JG. Polyploid tissues in the nematode Caenorhabditis elegans. Dev Biol [Internet]. 1985 [cited 2021 Mar 28];107(1):128–33.

Available from: https://pubmed.ncbi.nlm.nih.gov/2578115/

38. Altun, Z.F., Hall DH. Alimentary system, intestine. In: The Handbook of C elegans Anatomy In WormAtlas [Internet]. 2009 [cited 2021 Mar 28]. Available from: https://www.wormatlas.org/hermaphrodite/intestine/Intframeset.html

39. Delaney K, Strobino M, Wenda JM, Pankowski A, Steiner FA. H3.3K27M-induced chromatin changes drive ectopic replication through misregulation of the JNK pathway in C. elegans. Nat Commun [Internet]. 2019;10(1):1–15. Available from: http://dx.doi.org/10.1038/s41467-019-10404-9

40. Dudley NR, Labbé JC, Goldstein B. Using RNA interference to identify genes required for RNA interference. Proc Natl Acad Sci U S A [Internet]. 2002 Apr 2 [cited 2021 Mar 31];99(7):4191–6. Available from: /pmc/articles/PMC123624/

41. Santonicola P, Germoglio M, d'Abbusco DS, Adamo A. Functional characterization of Caenorhabditis elegans cbs-2 gene during meiosis. Sci Rep [Internet]. 2020 Dec 1 [cited 2021 Apr 20];10(1):20913. Available from: https://www.nature.com/articles/s41598-020-78006-w

42. Altun ZF, Hall D. Nervous System, General Description. In Worm Atlas. 2011.

43. Fang-Yen C, Alkema MJ, Samuel ADT. Illuminating neural circuits and behaviour in caenorhabditis elegans with optogenetics [Internet]. Vol. 370, Philosophical Transactions of the Royal Society B: Biological Sciences. Royal Society of London; 2015 [cited 2021 Apr 30]. Available from: http://dx.doi.org/10.1098/rstb.2014.0212

44. De Bono M, Maricq AV. Neuronal substrates of complex behaviors in C. elegans [Internet]. Vol. 28, Annual Review of Neuroscience. Annual Reviews ; 2005 [cited 2021 Apr 30]. p. 451–501. Available from: https://www.annualreviews.org/doi/abs/10.1146/annurev.neuro.27.070203.144259

45. Zhen M, Samuel AD. C. elegans locomotion: small circuits, complex functions. Curr Opin Neurobiol [Internet]. 2015 [cited 2021 Apr 30];33:117–26. Available

from: http://dx.doi.org/10.1016/j.conb.2015.03.009

46. Chasnov JR. The evolutionary role of males in C. elegans . Worm [Internet]. 2013 Jan [cited 2021 Apr 24];2(1):e21146. Available from: /pmc/articles/PMC3670456/

47. Cui, M. and Han M. Roles of chromatin factors in C. elegans development. In: Wormbook, ed The C elegans Research Community, WormBook, [Internet]. 2007. Available from: http://www.wormbook.org

48. Fields BD, Kennedy S. Chromatin Compaction by Small RNAs and the Nuclear RNAi Machinery in C. elegans. Sci Rep [Internet]. 2019 Dec 1 [cited 2021 Feb 25];9(1):1–9. Available from: www.nature.com/scientificreports

49. Cahoon CK, Libuda DE. Painting chromosomes in the nucleus. Elife. 2019;8:1–3.

50. WormBase : Nematode Information Resource. Gene: mes-3 [Internet]. [cited 2021 May 5]. Available from: https://wormbase.org/species/c_elegans/gene/WBGene00003221#0-9f-10

51. Justin N, Zhang Y, Tarricone C, Martin SR, Chen S, Underwood E, et al. Structural basis of oncogenic histone H3K27M inhibition of human polycomb repressive complex 2. Nat Commun [Internet]. 2016 Apr 28 [cited 2021 May 7];7(1):11316. Available from: www.nature.com/naturecommunications